Review Article

Kay Schuster*, Sonja Unger, Claudia Aichele, Florian Lindner, Stephan Grimm, Doris Litzkendorf, Jens Kobelke, Jörg Bierlich, Katrin Wondraczek and Hartmut Bartelt

Material and technology trends in fiber optics

Abstract: The increasing fields of applications for modern optical fibers present great challenges to the material properties and the processing technology of fiber optics. This paper gives an overview of the capabilities and limitations of established vapor deposition fiber preform technologies, and discusses new techniques for improved and extended doping properties in fiber preparation. In addition, alternative fabrication technologies are discussed, such as a powder-based process (REPUSIL) and an optimized glass melting method to overcome the limits of conventional vapor deposition methods concerning the volume fabrication of rare earth (RE)-doped quartz and high silica glasses. The new preform technologies are complementary with respect to enhanced RE solubility, the adjustment of nonlinear fiber properties, and the possibility of hybrid fiber fabrication. The drawing technology is described based on the requirements of specialty fibers such as adjusted preform and fiber diameters, varying coating properties, and the microstructuring of fiber configurations as low as in the nanometer range.

Keywords: Coating; fiber drawing; hybrid fiber; MCVD; multicomponent glass; technology; REPUSIL.

1 Introduction

Optical fibers have experienced a tremendous amount of success in optical communication during the last two decades. Today, more than 200 million km of fibers are produced annually. Optical communication networks provide the backbone of the modern information society. This success is based on the achievement of the successful development of extraordinary materials and the ability to tailor structural properties in modern optical fibers, mostly silica optical fibers. The concept of guided light gives light confinement its extremely high quality across almost unlimited lengths. The attenuation parameters achieved (e.g., as low as 0.17 dB/km in the 1550 nm wavelength band) are very close to the physical limits [1]. Dimensional structures are controlled into the sub-micrometer range in order to control mode behavior and dispersion properties. Complex cross-sectional structures of optical fibers, such as microstructured fibers or photonic band gap fibers, are carried out today using geometric fiber structures smaller than 100 nm [2].

In the context of optical fiber communication developments, further research fields have emerged. This includes especially fiber amplifiers [3], fiber light sources (fiber lasers, fiber supercontinuum light sources) [3, 4], and fiber sensor elements [5]. These application fields have triggered intensive research activities and provide great growth opportunities.

Such emerging application fields rely partially on the well-developed materials and technologies from communication fibers, but they also require new and adapted properties of optical fibers. The growing interest in such new application areas has, therefore, initiated research on new glass materials for optical fibers [6], as well as new material processing technologies [7] to overcome the limitations of current optical fibers. The desired functional properties concerning low attenuation in specific wavelength ranges [8], the variation of refractive index [9], the introduction of a highly nonlinear coefficient [10], or specific structural properties [11] are often well beyond the characteristics of the fibers that are currently available. There is also great interest in providing fiber structures from materials that cannot be drawn into optical fibers by conventional techniques.

In the sections that follow, we will present an overview of the current directions of research targeting the provision of a more extended range of materials and material combinations for use in guided light optics. Specifically, we will discuss different approaches in material and preform preparation, new gas phase doping methods,

---

*Corresponding author: Kay Schuster, Leibniz Institute of Photonic Technology (IPHT), Fiber Optics, Albert-Einstein-Str. 9, Jena 07745, Germany, e-mail: kay.schuster@ipht-jena.de
Sonja Unger, Claudia Aichele, Florian Lindner, Stephan Grimm, Doris Litzkendorf, Jens Kobelke, Jörg Bierlich, Katrin Wondraczek and Hartmut Bartelt: Leibniz Institute of Photonic Technology, Albert-Einstein-Str. 9, 07745 Jena, Germany

the concept of microstructured fibers, the fiber drawing process, and current developments in fiber coatings.

2 Preform technologies

The quality of an optical fiber is mostly defined by its preform. The preform fabrication methods can be classified into established methods mainly for telecommunication applications (such as the vapor deposition method and rod-in-tube technique) and into more unconventional methods for specialty fibers such as stack-and-draw, powder sinter and melt glass methods. In the following we will describe in more details three different methods applicable for modern types of specialty fibers. At the end of Section 2 the properties of these methods are summarized and compared in Table 4.

2.1 Preform preparation via vapor deposition methods

Vapor deposition methods have been proven to provide layered structures with excellent material quality and extremely low attenuation (e.g., as low as 0.2 dB/km). For the preparation of high silica fiber preforms the following methods have been developed [12–15]:

– modified chemical vapor deposition (MCVD)
– plasma-activated chemical vapor deposition (PCVD)
– outside vapor deposition (OVD)
– vapor axial deposition (VAD)

The MCVD and PCVD processes are inner vapor deposition methods. Here, the layers are deposited on the inside of a silica tube taking advantage of an oxidation process. The chemical reaction is initiated by a burner, or furnace, in the MCVD process, and by a microwave plasma in the PCVD process. In contrast, in the OVD and VAD processes, layer deposition is carried out on the outside of a rotating mandrel using the flame hydrolysis technique. These vapor deposition methods differ in the deposition rate and efficiency, in the precision of refractive index profiles and in the possible dimension of the preform. The OVD and VAD processes permit the fabrication of very large preforms. In the PCVD process, the deposition rate is low but the deposition is much more efficient than in the other processes.

We will concentrate in the following section on the description of the MCVD technology as a typical example for these vapor deposition methods.

2.1.1 The MCVD process

MCVD technology is the most common fabrication method for passive and active optical fiber preforms [15]. This process is schematically shown in Figure 1 and characterized by the following details.

Halides are entrained in a gas stream in controlled amounts either by passing a carrier gas such as oxygen (O_2) through liquid dopant sources or by using gaseous dopants. These high purity halide compounds (such as $SiCl_4$, $GeCl_4$, $POCl_3$, BBr_3, BCl_3, SiF_4, SF_6...) have high vapor pressures at room temperature. The gas mixture is passed through a
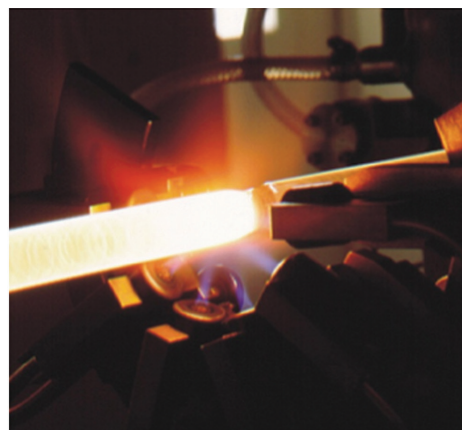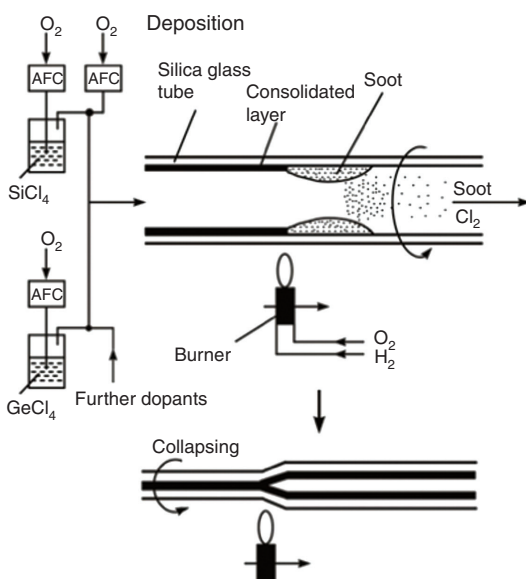
Figure 1 Schematic of the MCVD process.

rotating quartz glass tube and (RE oxidized in the hot zone of a hydrogen/oxygen (H_2/O_2) burner from the outside at a temperature of about 1800°C. The (doped) SiO_2 particles are deposited in the form of fine soot on the inner surface of the tube just ahead of the burner (thermophoretic deposition). This soot is subsequently consolidated into a clear glass layer using a moving burner. The burner is continuously shifted back and forth across the length of the tube, and the layers are gradually deposited, the first cladding layers at a refractive index of SiO_2 or lower and the following core layers at a higher refractive index. Finally, the tube is collapsed at very high temperatures of above 2000°C in several steps under a chlorine (Cl_2) atmosphere to a cylindrical rod (preform). If necessary, this primary preform is jacketed with a further quartz glass tube to achieve a defined core-to-cladding ratio and then drawn into a fiber.

The thickness of the deposited layers can be varied between 5 µm and 100 µm as a function of the $SiCl_4$ flow rate. The amount of dopants and the corresponding refractive index change (Δn) are determined by the flow rate of the dopant halides. Dopants such as germanium (Ge) and phosphorus (P) increase, whereas dopants such as boron (B) and fluorine (F) decrease, the refractive index of silica.

By varying the dopants and their concentrations, it is possible to obtain well-defined refractive index profiles (step index or graded index) for single-mode or multimode propagation properties.

In the high temperature process, dopant incorporation in silica is determined and significantly influenced by:

– equilibrium thermodynamics (such as for Ge, F, and P incorporation [15, 16])
– evaporation of the dopants through lower oxide formation (GeO, PO_2, BO_2...) and in the case of fluorine doping largely through SiF_4 formation during the deposition and collapsing process
– strong interaction of the dopants with fluorine under formation of volatile fluorine components (as GeF_4, BF_3...[17])
– diffusion processes

The real concentration and refractive index profiles in the preforms and fibers are always diffusion influenced profiles. Therefore, under the influence of the high temperature (2000°C–2300°C) collapsing process, evaporation is supported by a high diffusion rate that takes place even on consolidated layers, leading to the well-known 'dip' in the preform center. Knowledge of the diffusion coefficients of the dopants is important to understand and optimize the process. Therefore, over a span of several years the diffusion behavior of different dopants (such as OH, Cl, F [18], P [19], Ge [20], B [21]) in silica depending on the temperature (1600°C–2000°C) and dopant concentration was investigated.

The MCVD process is an extremely flexible technique for implementing varied fiber structures and compositions, but it causes disturbances due to the nature of the process. Figure 2 shows typical refractive index profiles for different kinds of passive preforms.
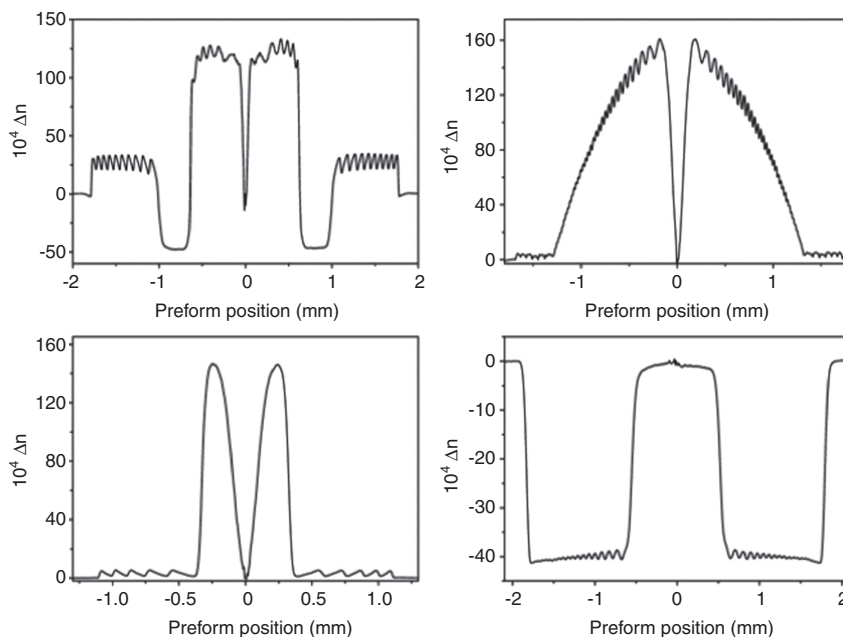

Figure 2 Typical refractive index profiles of prepared passive preforms via the MCVD process.

2.1.2 Solution doping for rare earth and aluminum incorporation

The passive fiber structures discussed above are widely used in fiber communication and fiber sensor applications [13]. For active fiber devices such as fiber lasers and fiber amplifiers, rare earth (RE)-doped fibers are required. Here, the fiber core is doped with RE ions [such as neodymium (Nd), ytterbium (Yb), erbium (Er), or thulium (Tm)]. However, the option of incorporating these RE ions in silica is limited, and it is difficult to achieve a high doping level of such ions. By adding codopants such as aluminum (Al) and/or phosphorus (P), the solubility of RE ions in silica can be improved and thus the RE content increased without phase separation and crystallization.

In contrast to silica and the common dopants Ge, P, B, and F, volatile precursor compounds do not exist for the RE dopants and the most important codopant Al that can be vaporized at or slightly above room temperature. Therefore, as one option, they are supplied via a liquid phase. This method, so-called solution doping, in combination with the common MCVD process, is the most widely used and successful technique [22]. The active core deposition is achieved in the following way.

After the preparation of an inner tube layer, which is not fully consolidated during the MCVD burner pass, the porous layer is impregnated with an aqueous or alcoholic solution of RE and Al salts (well-soluble chlorides or nitrates) and dried. The solid salts remain in the porous silica structure. During subsequent high temperature treatments, the silica is consolidated to a fused glassy layer and the salts are converted to RE and Al oxides and incorporated into the silica matrix. The amount of Al and RE incorporated is determined by the relative density of the porous layer and the solution concentration of Al and REs [23]. This process is very flexible and permits the incorporation of all RE elements.

The codopants influence both the preparation process and the fiber properties in a manifold and complicated manner. Thus, the codopants influence the RE incorporation and diffusion, the refractive index profile and glass devitrification, the laser properties, and the optical background losses of the fibers. Diffusion processes during preparation determine the refractive index distribution, geometry, and the numerical aperture of the preform core. Knowledge of these strong interactions between REs and codopants is very important for the successful fabrication of defined fiber core compositions for high-efficiency laser fibers. For years, the influence of codopants on several aspects such as the following has been intensively investigated:

- diffusion behavior of RE ions [24]
- concentration and refractive index distributions [25–29]
- absorption and emission properties from UV to NIR [25–29]
- photodarkening [30–35]

Based on these investigations, the deposition process and core composition have been optimized for the manufacturing of active single or low-mode fibers with low background loss, high efficiency, reliability, and beam quality to be used in the wavelength range of 1 μm–2 μm. In Table 1 different types of high silica RE-doped fibers (with RE ions, codopants, emission wavelength) prepared using the MCVD/solution doping technique are summarized.

Ytterbium, Ce-doped alumosilicate laser fibers are distinguished by low photodarkening and high power stability. Output powers in the multi-kW range have already been successfully demonstrated [29, 30].

2.1.3 Gas phase doping for REs and aluminum incorporation

MCVD/solution doping technology has several limitations concerning the geometry, doping and refractive index homogeneity, and the incorporation of very high RE and Al concentrations (in excess of 2 mol% RE_2O_3 and 7 mol% Al_2O_3). For example, this technique only permits the deposition of cores that possess an excellent optical quality of up to a diameter of about 1.5–2 mm. The implementation of large core/cladding ratios is also limited. Therefore, new techniques are being developed to enable the deposition of RE and Al in the gas phase of the MCVD process and ultimately overcome the limitations in geometry and homogeneity. To this end, solid precursors of metal organic complexes of RE [such as RE-(tetramethylheptanedionate)$_3$) and Al (such as Al-(acethylacetonate)$_3$] or Al chloride ($AlCl_3$) are converted to gas phase via high-temperature evaporation, as first reported in 1990 by Tumminelli et al. [36]. The so-called

Table 1 Types of high silica RE-doped fibers.

RE ions	Codopants	Emission wavelength (μm)
Nd^{3+}	Al	1.0–1.1
Yb^{3+}	Al	
	Al, P	1.0–1.1
	Al, Ce	
Er^{3+}	Al, Ge	1.5–1.6
Er^{3+}/Yb^{3+}	P, Al	1.5–1.6
Tm^{3+}		
Ho^{3+}	Al	1.7–2.1
Tm^{3+}/Ho^{3+}		

MCVD/chemical in crucible technique was developed at the Optoelectronics Research Centre (University of Southhampton) [37]. Here, the evaporation of the precursors is carried out in an electrically heated crucible directly within the quartz glass process tube following deposition together with silica and common dopants. The advantage of this setup is the closely spaced evaporation of the RE precursor and the reaction zone: precursor delivery lines are not necessary, nor do problems with the condensation of precursors inside the lines occur. However, it is not possible to produce defined vapor mixtures of several precursors (e.g., the combination of Al and Yb) because of the different evaporation temperatures. Instead of this method, delivery of the gaseous precursors takes place from external chemical sources. This vapor system is commercially available and successfully used in some facilities [38–41] for the preparation of active fiber preforms.

The latter described gas phase doping process for the active core layers (described here for Yb and Al doping) is shown in Figure 3 and is characterized by the following steps: The solid starting materials, which are placed at several plates in separate evaporators, are vaporized (carried out in a cabinet) at temperatures of 130–14°C for $AlCl_3$ and 190–200°C for Yb-(tetramethylheptanedionate)$_3$ [Yb(tmhd)$_3$], respectively, to achieve an acceptable vapor pressure. The gaseous precursors are delivered together with the carrier gas helium (He) and additional oxygen (O_2) separately through heated lines to the inside of the quartz glass process tube and mixed there with the other common gaseous halides (such as $SiCl_4$, $GeCl_4$, $POCl_3$...).

To prevent condensation of the precursors inside the lines, the cabinet and all lines (from evaporation to injection into the quartz glass tube) must be heated above the evaporation temperatures of about 200°C. Deposition, consolidation, and collapsing into the preform are carried out in the usual manner as described in detail in Section 2.1.1.

The incorporation of the dopants Yb and Al is dependent on the process parameters (such as evaporation temperatures, gas flows, collapsing conditions). Compared to the MCVD/solution doping method, it is possible to prepare efficiently large cores through the continuous deposition of several layers. However, at present it is difficult to incorporate all RE elements with sufficient concentration because of the absence of suitable precursors (such as for Ce). Furthermore, these gas phase techniques are less established and investigated compared to the MCVD/solution doping method due to the critical process control.

Our first own systematic investigations were started with the incorporation of Yb and Al. Using the procedure described above, preforms and fibers were prepared according to the process parameters (such as evaporation temperatures, gas flows, collapsing conditions) in a wide range of Yb and Al concentrations resulting in a preform core diameter of about 2 mm. The prepared samples show an excellent radial uniformity concerning the refractive index and dopant concentration distribution (see Figure 4A). The cross section of the preform core is depicted in Figure 4B. The image was taken using backscattered electrons, in which the brighter area gives a visual impression of the Yb, Al-doped preform core. In
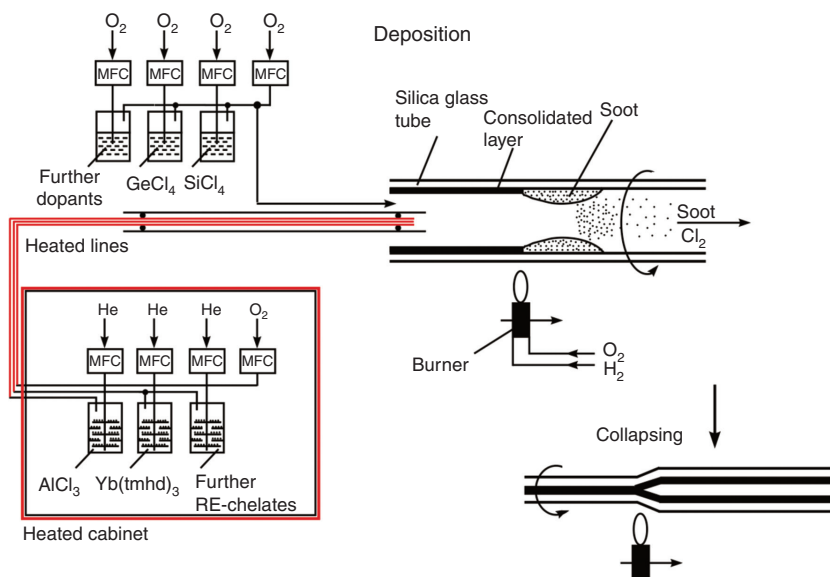

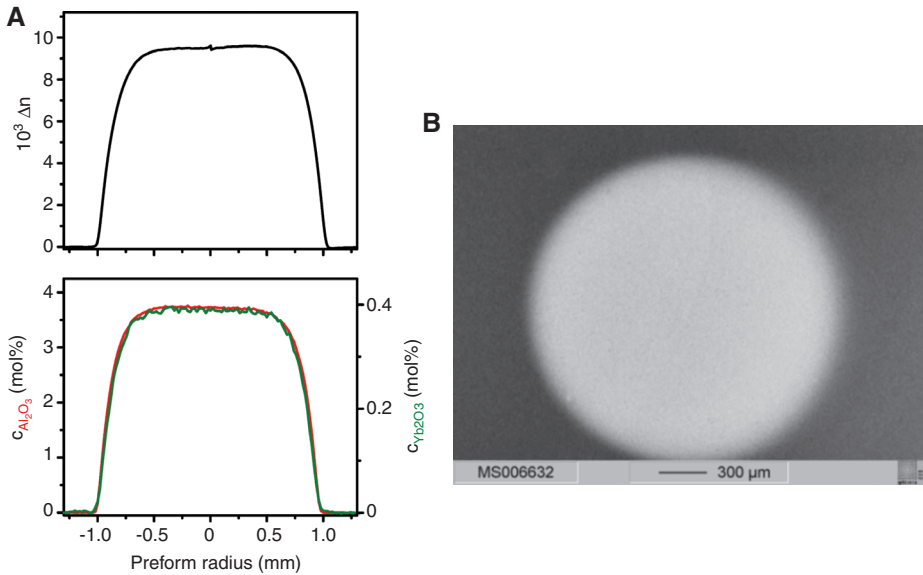**Figure 3** Schematic of the MCVD process combined with gas phase doping for RE and Al.

Figure 4 Radial refractive index and concentration profiles of an Yb, Al-doped silica preform (A) and cross section of a preform core shown by backscattered electrons (B).

contrast to the MCVD/solution doping process, a very high doping level of Al of up to about 16 mol% Al_2O_3 was already achieved with good uniformity of the refractive index and dopant concentration distribution [38, 40].

The absorption and emission properties investigated in the UV/VIS/NIR region are comparable to preforms and fibers made using the MCVD/solution doping technique. Laser experiments have demonstrated fiber laser properties with an excellent slope efficiency of 80% and output powers of about 200 W comparable to fibers prepared using MCVD/solution doping and the REPUSIL technique [41].

Our own prepared Yb, Al-doped fibers have not yet been optimized in terms of minimizing pump-induced losses (photodarkening effect). Therefore, the incorporation of Yb together with P and Al is currently being investigated in order to produce low NA fibers with low photodarkening comparable to fibers prepared using MCVD/solution doping [31]. Intensive investigations, concerning the Al/P codoping, were already undertaken by Bubnov et al. [38]. Other research works also concentrate on the deposition of larger preform cores (diameter >3 mm) that have already been achieved [39, 40].

2.1.4 Powder sintering methods for the preparation of fiber optic preform materials

MCVD and other gas phase processes can produce doped silica glasses with excellent properties in reference to purity, dopant type, and dopant level. Such layer-based preparation technologies suffer, however, from fundamental limitations in the implementation of homogeneous volume materials. Recently, a new technology for the preparation of doped glasses based on a powder sintering method has been developed in cooperation with the Heraeus Quarzglas Company [42–44]. This preparation method, the so-called REPUSIL process, can be considered as a modification of the solution doping process for production of the Al/RE-doped silica layer for fiber preforms. However, the doping and purification process is achieved outside the silica tube by using a suspension-doping step. Because of this outside step, larger amounts of uniformly doped silica can be produced. Starting materials for the REPUSIL process are high-purity gas phase-formed silica nanoparticles and water-soluble compounds of the doping components, e.g., $AlCl_3 \times 6H_2O$, RE chlorides and ammonium tetra borate. Defined amounts of the doping solution are mixed into a silica suspension under controlled adjustment of the pH value. As a result, the doping ions are precipitated as pure ore mixed hydroxides on the surface and in the pores that are intrinsically tied to the suspended silica particles. After drying the doped solution, a moldable granulate is produced with the help of isostatic pressure mostly in cylindrical shapes. Next, this porous green body is purified by chlorine at elevated temperatures to remove impurities from raw materials like iron, other 3d elements and, most importantly, bonded water. These cleaned glass precursors are fed into a matched fused silica tube. With the help of typical MCVD equipment, the doped, but not yet glassy silica body, is then transformed into transparent glass samples of up to 50 g in weight.

The sintering and vitrification process is carried out at temperatures of up to 2200°C and is controlled by different adapted runs of an oxygen hydrogen burner. An electrical furnace with a very small heating zone can be used for this step of the process as well. Figure 5 shows a schematic of the described process.

Many modifications are available for this process. The prepared glass can be used directly for fiber drawing, or the undoped silica tube can be removed by grinding. Also, pure doped glass is available as rods for stack and draw technology for microstructured fiber preforms. The concept of powder sintering technology is also of special interest in providing fluorine-doped glasses (reduced refractive index) since it is difficult to incorporate larger fluorine amounts homogeneously via the classic MCVD solution doping process. Here, large losses in fluorine by diffusion and evaporation during the high temperature step were observed. The control of fluorine incorporation in alumina and RE-codoped glasses enables new fiber optic applications, especially in the development of large-core fiber lasers with the highest brightness. Figure 6A shows the refractive index profile of a pure Al and SiF_4
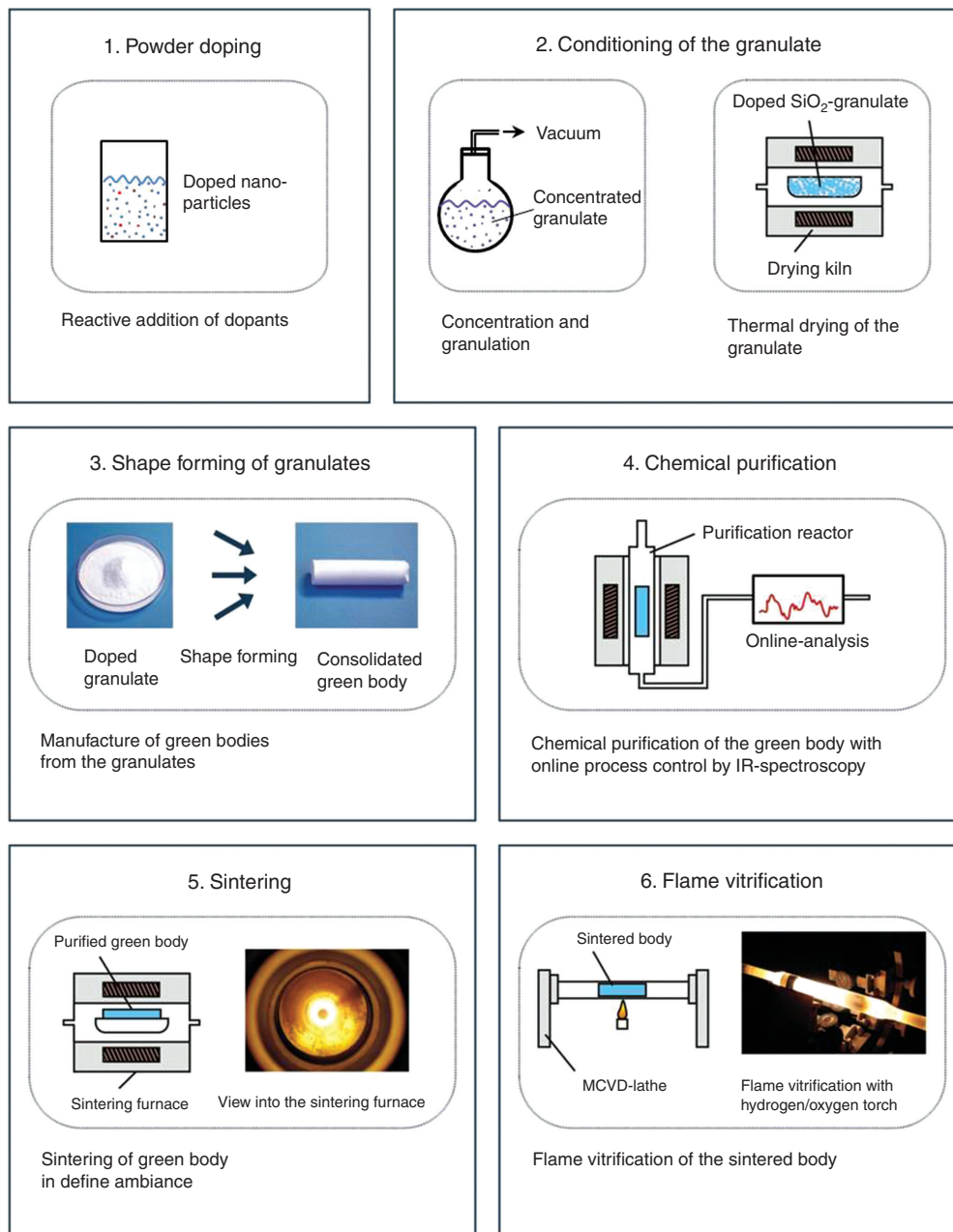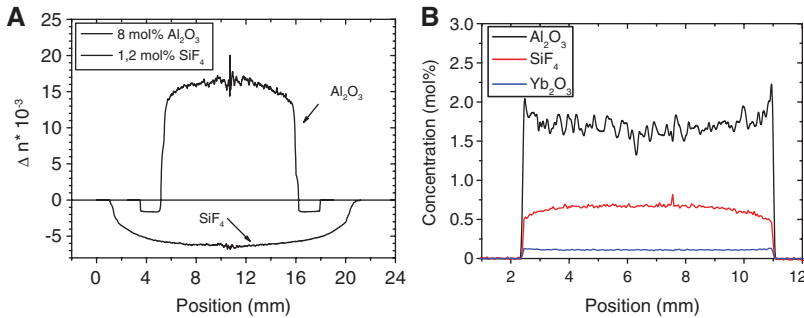

Figure 5 Schematic of the REPUSIL process.

Figure 6 Index profile of two different doped bulk materials: the current limits in high-index REPUSIL materials (Al_2O_3 doped) and low-index REPUSIL materials (fluorine doped) are shown (A), concentration profile (WDX) of doped bulk REPUSIL materials (B).

bulk glass, whereas Figure 6B depicts, as an example, the concentration profiles of Al/Yb bulk glass with fluorine incorporated. At present, the following parameters for high-purity doped silica glasses can been achieved following the REPUSIL process:

– content of alumina: 0–8 mol%
– content of RE oxide in combination with aluminum oxide: 0–0.6 mol%
– content of boron oxide in combination with aluminum oxide and RE oxide: 0–10 mol%
– best attenuation (fiber loss) in Al-Yb doped at 1200 nm: 15 dB/km.
– fluorine content (as mol% SiF_4): 2.0 mol% SiF_4 in pure silica, 1.8 mol% SiF_4 in Al/RE
– doped silica

The REPULSIL process has been shown to provide similar fiber laser efficiencies as fibers produced by the MCVD/solution doping technology (Figure 7). The possibility of producing larger fiber cores with the REPULSIL process in combination with very uniform refractive index profiles will enable further power scaling.
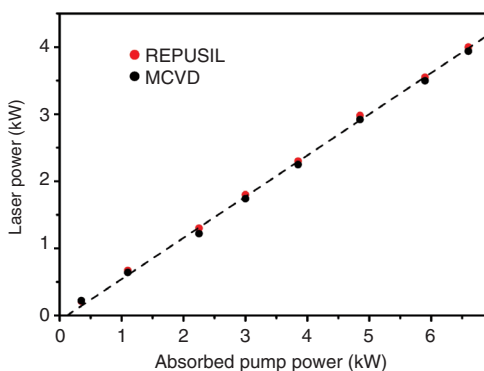

Figure 7 Fiber laser characteristic of Yb, Ce-doped alumosilicate fibers prepared using MCVD/solution doping and the REPUSIL technique. (Measured by G. Rehmann, Laserline GmbH).

For future investigations, the incorporation of phosphorous oxide in combination with alumina and RE oxides is of interest. Phosphorous-doped silica is a very suitable base material for high-power fiber laser applications. These types of glasses show the lowest photodarkening values in Yb-doped fiber lasers. In the case of an Al/P molar ratio of 1, a change in the refractive index cannot be observed for different amounts of Al/P. The extraordinary properties of this combination of dopants make it possible to implement LMA fiber designs with an extremely low-index step for the best fiber laser performance. An overview of potential application fields for such powder-based bulk silica glasses is shown in Table 2, and examples of fiber structures based on rods made using powder sintering technology are shown in Figure 8.

2.2 Glass preform preparation via crucible melting technology

In order to provide a large selection of glass material with different properties, classical melting technologies also have to be applied. The MCVD and powder sintering technologies discussed above are not applicable for all types of glasses. In addition to simple manufacturing, the significant advantages of a crucible melting technology over the MCVD and REPUSIL processes include the implementation of high dopant contents in melted glass, an easy volume scaling, and the good optical glass quality as a consequence of the high melting homogeneity. Based on crucible melting technology, the possible compositions of high silica glasses can be expanded significantly. By adding additional dopant components like fluorine and other RE elements (e.g., Yb, Tm, and Er), the thermal and optical properties of these glasses can be adjusted across a wide range. The glasses can be processed to fiber preforms, tubes, rods, and plates by applying specific melting

Table 2 Benefits of high-purity doped bulk silica glass (REPUSIL) for fiber application.

Doping agents	Benefits	Applications
Al_2O_3 0–8 mol%	High refractive index change Better UV transmission than germanium Lower strain than germanium	LMA transport fiber with high NA and large spectral range for pump light in laser equipment Pedestal fiber structures
SiF_4 0–2 mol%	Homogeneous fluorine-doped bulk silica glasses Refractive-index depressed material	Silica-silica based fiber Fiber for UV range High NA fiber
Al_2O_3/Yb_2O_3 0–6 mol%/ 0–0.6 mol%	Bulk materials of doped silica with high purity and homogeneity Low coast glass in contrast to MCVD material	High-power fiber laser up to 6 kW, CW run Short pulse fiber laser with LMA core
B_2O_3 0–10 mol%	Bulk materials with extraordinary homogeneity Low coast glass in contrast to MCVD material Codopant for refractive index adaption	Stress elements for polarization-maintaining fiber Refractive index compensation
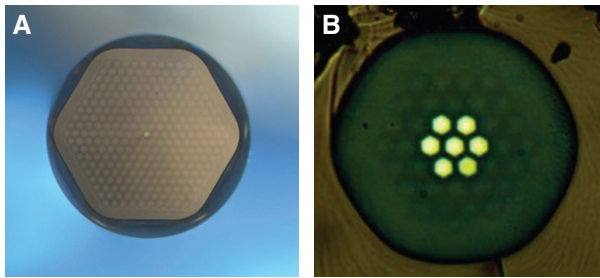
Figure 8 Extra-large mode area (X-LMA) fiber with 50 μm core and 1.2 mm outer diameter (A), multi-core fiber for pump absorption optimization (B).

and casting techniques. These melted glasses are of great interest for a series of applications, such as for use as bulk, rods and fibers in lasers [45] and nonlinear devices [46].

A major challenge in the fabrication of active and passive optical fibers based on melted glass is the combination of different glass types in the fiber preform, e.g., highly doped silicate glass as a light-guiding core material with an ultra-pure fused silica cladding. The combined drawing of silica and silicate glasses (SiO_2 content <70 mol%), or other materials, requires an optimized glass composition with regard to transformation temperature, expansion coefficient, and diffusion effects. A suitable candidate for such material combinations is the SiO_2-Al_2O_3-La_2O_3 (SAL) glass system based on investigations presented in Hyatt and Day [47], Shelby et al. [48], and Dejneka [49]. The good melting behavior, high redox stability and a sufficient solubility of RE elements in glass make these SAL glasses very suitable for fiber applications. The potential of these glass materials for combination with a SiO_2 cladding allows a refractive index difference between the core and the cladding of up to 0.1. Numerical apertures of up to 0.55 can be achieved (see also Section 3.3.2). Investigations into SAL glasses, such as glass preparation and characterization of material properties, are described in [50]. Glass types with a high SiO_2 content are used (high silica glasses, 65–70 mol% SiO_2) since they permit significantly higher concentrations of both active RE (e.g., Yb) and codopants. Lanthanum and aluminum are the codopants in this case and a high fraction of aluminum (e.g., 20 mol% Al_2O_3) enables a very good solubility for RE ions. The easy substitution of lanthanum with other RE elements allows a great variability in glass properties [50, 51]. One challenge is the preparation of glass compositions for fibers with low attenuation and the feasibility for a fiber drawing process without degradation of the optical properties.

2.4 x 2.4 x 12 cm   ∅=20 mm   ∅= 20/4 mm
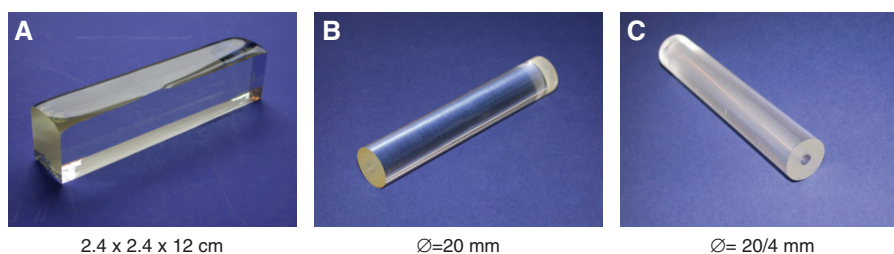
Figure 9 SAL glass block after fine cooling (A), grinded and polished SAL preform (B), and SAL tube (C).

Samples of SiO_2-Al_2O_3-La_2O_3 glasses were fabricated using high-quality (3N-5N) raw oxide materials (SiO_2, La_2O_3, Yb_2O_3, CeO_2) and hydroxide [$Al(OH)_3$]. For homogenization, the liquid glasses were fritted in ultra-pure water, dried, and subsequently re-melted at 1650°C whilst stirring. After several hours of melting, the liquid glass was poured into a stainless steel mold to form glass blocks (Figure 9A). The blocks were slowly cooled down from T_g to room temperature at 100K/h. Following this fine cooling procedure, the homogeneous, bubble-free blocks were ground and polished into a cylindrical shape (Figure 9B and C) to be used as preforms for fibers and as rods in microstructured preforms (see also Section 3.3.2).

The SAL glass compositions can be optimized in terms of thermal and optical requirements for both a high lanthanum and aluminum concentration and good compatibility with a silica cladding. The glass-forming region and glass stability of the SAL system are influenced and limited by the RE_2O_3 (e.g., RE=La, Yb) concentration. SAL glasses show a high transition temperature, which is a great thermochemical advantage with regard to their combination with pure silica glass. SAL glasses with a high lanthanum content exhibit a high refractive index and a nonlinear coefficient twice as high as that of SiO_2 and are suitable for nonlinear applications (e.g., supercontinuum generation). The partial substitution of lanthanum with ytterbium as an active dopant enables the fabrication of glasses and fibers for laser application (e.g., for high power operation). In Figure 10, the Yb^{3+} typical absorption and emission spectra of the melted SAL glasses are shown. The absorption and emission spectra, as well as the lifetime of the Yb-doped SAL glasses, are very similar to those known from Yb^{3+} in Al_2O_3/SiO_2 glasses produced via MCVD. In Table 3, the important thermal properties
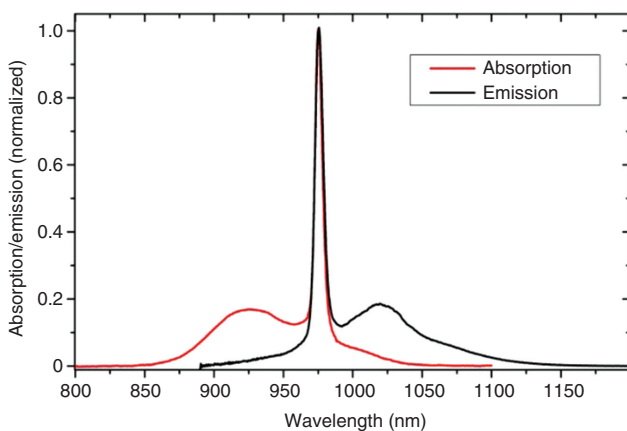

Figure 10 Absorption and emission spectra of an Yb-doped SAL glass.

Table 3 Overview of thermal properties and refractive indices of melted SAL glass – with and without Yb_2O_3 – compared with commercial pure silica glass (Heraeus, Suprasil F300; Heraeus Quarzglass GmbH & Co. KG, Kleinostheim, Germany).

Glass composition range (mol%)	SAL glass	SAL glass Yb-doped	Pure silica glass
SiO_2	55–70	66–70	100
Al_2O_3	15–20	21–23	
La_2O_3	10–24	3.6–11.0	
Yb_2O_3		0.1–6.0	
Transition temperature Tg (°C)	861–875	867–884	1120
Thermal expansion coefficient α (10^{-6}/K)	4.3–7.0	4.0–4.6	0.5
Refractive index @ 633 nm	1.60–1.74	1.60–1.61	1.456

and refractive indices of prepared SAL glasses – with and without Yb_2O_3 – are summarized. Table 4 shows a comparison of the described preform fabrication methods regarding possible active doped material quantities and selected optical properties.

3 Fiber fabrication and coating technologies

3.1 The fiber drawing process

Optical glass fibers are prepared from preforms by a fiber drawing process at temperatures adjusted to near the softening point of the glasses used. The drawing process can basically be carried out according to two different methods: either by directly drawing the glass fiber from molten glass or by continuously drawing from the neckdown region of a partially softened fiber preform [52]. In the direct-melt process, pieces of multi-component glass are placed into two concentric crucibles (double-crucible method [53]) and combined in a molten state to form the fiber core and cladding layer. The continuous drawing is outlined in this section. A schematic overview of this process is shown in Figure 11.

Today, optical fibers are typically fabricated in a vertical drawing process from a solid unstructured or structured glass preform (i.e., core-cladding structure), which offers a wider range of fiber design alternatives [54]. Advanced modular fiber drawing equipment mainly consists of different functional components, such as a preform fixing and feeding unit and a high-temperature furnace in the upper part of the system, followed by coating applicators, coating curing units, a fiber-pulling capstan, and a winding device with a traversing spool to take up the

Table 4 Comparison of preform fabrication methods regarding possible quantities (RE doped materials) and relevant material and fiber properties.

Method	Active doped core materials			Fiber	
	Quantity	Max. doping level RE/codopants	Homogeneity/refractive index fluctuation	Core/cladding ratio	Background loss
MCVD/solution doping of RE and Al	2 g Preform Length: 300 mm Diameter: 2 mm	2 mol% RE_2O_3 (all RE ions) 7 mol% Al_2O_3 20 mol% P_2O_5 30 mol% GeO_2	Fluctuation depending on the codopants and Doping concentration dip: P, Ge codoping	< 0.2	<10 dB/km
MCVD / gas phase doping of RE and Al	15 g Preform Length: 300 mm Diameter: 5 mm	0.8 mol% Yb_2O_3 0.8 mol% Er_2O_3 0.2 mol% Nd_2O_3 0.06 mol% Tm_2O_3 15 mol% Al_2O_3 20 mol% P_2O_5	Yb/Al doping: excellent radial uniformity dip: P, Ge codoping	≤0.5	15 dB/km
REPUSIL	200 g	0.6 mol% RE_2O_3 (RE=Yb, Tm, Ce) 8 mol% Al_2O_3 1.8 mol% SiF_4 10 mol% B_2O_3 1 mol% P_2O_5	RI fluctuation in very short range order (μm scale)(bulk: μm scale, fiber: nm scale)	≤1.0	15 dB/km
Molten glass technique (SAL glass)	15 kg	15 mol% La_2O_3 6 mol% Yb_2O_3 0.9 mol% RE_2O_3 (RE=Ce, Pr, Eu, Tb, Er, Tm) 23 mol% Al_2O_3 4 mol% AlF_3	concentration-striae (from glass bulk) diffusion process (during fiber drawing) RI fluctuation in long range order (mm scale)	≤1.0	500 dB/km

fiber continuously at the lower end of the drawing line. An appropriate number of non-contact laser diameter measuring heads (2-axis or 3-axis heads) monitors the vertical fiber position and diameter of the pristine bare glass fiber after leaving the furnace, and the diameter of the coated fiber. This diameter measurement allows continuous inline control and adjustment of the diameter during the fiber drawing process. To achieve a desired fiber diameter, the measured diameter values are fed into a closed control loop that instantaneously adjusts the necessary drawing speed.

Optionally, a caterpillar capstan can be installed in line with the drawing system, which is designed to pull glass rods, thin-walled capillaries, or sub-structured canes with minimal surface pressure. All these devices are aligned vertically along the drawing line in a mechanically stable tower that is usually higher than 4 m. Larger heights (e.g., >20 m) are necessary for high-speed fiber drawing [55] at drawing speeds of >1000 m/min in order to provide sufficient fiber cooling across the distance

between the furnace outlet and coating applicators. Appropriate fiber cooling is necessary to prevent overheating the coating material from contact of the coating material with a high-temperature fiber, which can result in improper wetting.

A draw tension gauge can also be installed at the preform feeder or at the fiber capstan to monitor the fiber draw tension. The draw tension is influenced by different drawing conditions such as furnace temperature and preform and fiber diameter, and is linearly related to the fiber draw speed [56]. A high draw tension leads to an increase in optical fiber loss and to degradation of fiber strength due to the fatigue effect [57]. In order to prevent the glass fiber from breaking during drawing and to avoid the manufacture of extremely weak glass fibers, the drawing force at a conventional fiber diameter of 125 μm at low draw speeds of about 5 m/min to 50 m/min should not exceed 1.2 N (corresponding to a drawing tension of 1.47×10^{-8} N/m^2 for a 125 μm diameter fiber) regardless of the preform dimension.
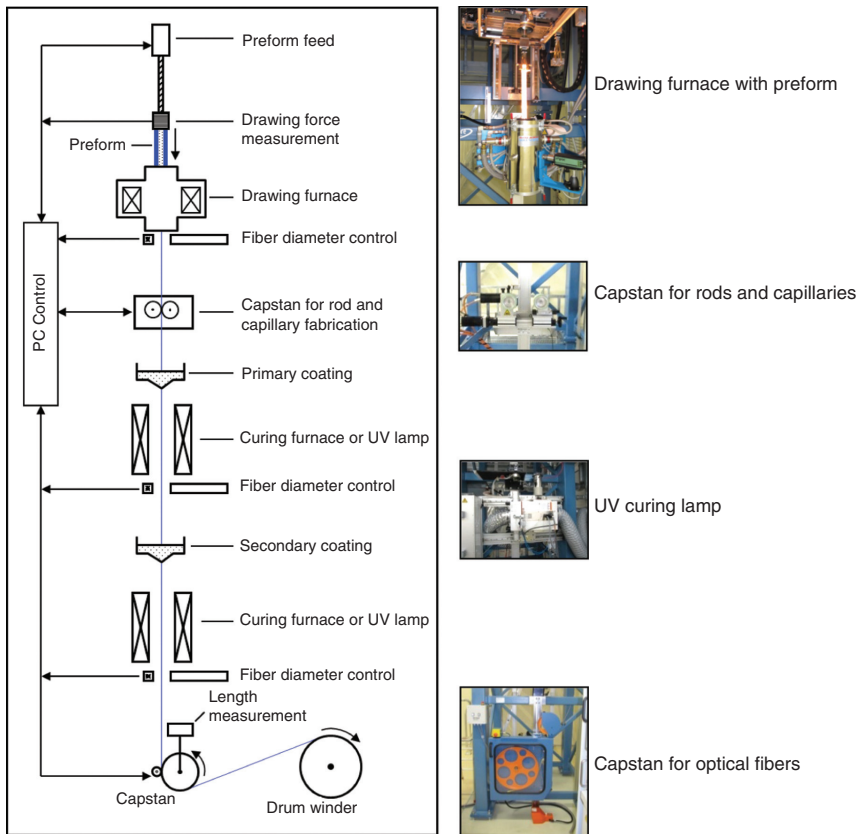
Figure 11 Schematic drawing set up for optical fibers.

The theoretical length of a fiber that can be drawn from a given preform, as well as the required drawing speed, can be derived from the law of mass flow conservation. At a given preform diameter d_p and preform feed rate v_p, the required fiber drawing speed v_f to achieve a desired fiber diameter d_f can be calculated by the following equation:

$$v_f / v_p = d_p^2 / d_f^2 \tag{1}$$

The length of an optical fiber l_f that can be drawn from one preform with length l_p depends on its volume and is determined by a similar equation using $v_f=l_f/t$ and $v_p=l_p/t$:

$$l_f / l_p = d_p^2 / d_f^2 \tag{2}$$

The ratio between the preform and fiber diameter d_p^2/d_f^2 is called the draw-down ratio.

The fiber drawing process is started by inserting the fiber preform into a drawing furnace at the top of the tower and heating up the preform glass close to its softening temperature. Both graphite and zirconia-based furnaces (i.e., resistant and inductive heating, respectively) with precision temperature controllers are the most commonly used electric drawing furnaces. Graphite furnaces must be operated under an inert gas atmosphere (typically argon or helium gas) to prevent oxidation of the graphite components (muffle, heating element, and liner tube) [58]. The temperature distribution in the heating zone of the drawing furnace determines the temperature gradient across the preform diameter and thus influences the formation of the neck-down region and consequently the arising fiber drawing tension.

Depending on the processed glass material, the preform dimensions, and the structure, the fiber preform softens at temperatures of up to 2000°C to form a neck-down region at its tip, which is reduced under the force of gravity to the desired fiber diameter.

Next, the optical fiber is coated with a coating layer by passing it through a series of coating applicators after leaving the drawing furnace. The coating system consists of coating dies (pressurized die or gravity die) containing the liquid coating material and also features curing units, such as UV lamps for ultraviolet-radiation curable materials (e.g., acrylate-based resins, polyurethane, ORMOCER®) or furnaces for thermally curable materials (e.g., silicone, polyimides). The coating concept for optical fibers is discussed in more detail in Section 3.2.

Finally, the glass fiber with coatings is pulled down along the drawing line and continuously wound on a traversing winding drum.

Some of the typical parameters are presented in the following to illustrate the drawing process. The most common material for optical fibers is pure silica and doped silica glass. Depending on the doping level, the softening range of high silica glasses extends from 1700°C to 2350°C. The viscosity of silica glass at a temperature of 1935°C–2322°C varies from $10^{4.86}$ Pas to $10^{3.63}$ Pas [59]. During the drawing process, the preform is slowly moved through the heating zone at a rate of usually less than 1 mm/min while the glass fiber is continuously drawn much faster in the m/min region. The exact velocities are determined by the draw-down ratio. Research drawing towers usually have a drawing speed capability of ≤200 m/min whereas industrial drawing towers allow for fiber drawing speeds of up to 1200 m/min.

It should be noted that typical fiber performance characteristics such as optical fiber loss and fiber strength are partly influenced by the drawing conditions. For example, transmission loss depends on the draw tension. It was shown that in doped silica core fibers (Al-Ge-Yb-doping) the optical loss decreases significantly with increasing fiber tension. As mentioned above, the fiber draw tension has a linear relationship with the drawing speed and is also dependent on the furnace temperature and the draw-down ratio [55].

The fiber strength is directly affected by the composition of the fiber structure (core and cladding materials and geometries) as well as by the fiber cooling rate and draw tension. The cooling rate is basically determined by the fiber diameter and drawing speed – smaller diameter fibers tend to show higher strength than larger fibers. During the drawing and fiber cooling process a mechanical stress (tensile or compressive stress) is induced in the fiber structure, which will partially remain as residual stress affecting the fiber strength [56]. Depending on the preform material, the dwell time of the preform in the hot zone of the drawing furnace can initialize surface or bulk crystallization. This can be prevented by an increased preform feed rate and by a modification of the internal furnace gas atmosphere.

3.2 Coatings for optical fibers

Coatings for optical glass fibers do not necessarily influence the optical properties but are nevertheless necessary to i) preserve the mechanical strength of pristine fibers by protecting them from moisture and mechanical impact (prevention of microbending, protection from hazardous environments) and ii) ensure optical performance of fibers (adjustment of fiber numerical aperture, decrease in optical loss, mode stripping, etc.). In addition, the fiber coating might address other functional aspects, such as electrical or thermal conductivity or transmission of mechanical stress parameters from embedding media in the fiber (e.g., mechanical sensing) [60–63].

Three different classes of coatings are available on the market for glass fibers: organic, inorganic, and hybrid coatings. The organic coating material includes ultraviolet (UV) curable resins and thermally curable resins. Commonly used organic coatings include perfluoro polymers (e.g., Teflon), polyacrylates, polyimides, silicones and their derivatives. Among the acrylic polymer coatings, fluorinated formulations are available that have a refractive index below that of the silica glass material itself. Such low index coatings are of particular interest for laser applications in which a high fiber numerical aperture (NA >0.45) is required. Hybrid coating materials for optical fibers are based on organically-modified ceramic precursors (ORMOCER®s) and combine the properties of organic and inorganic components. Such hybrid materials are applied where properties of both polymers and inorganics are required (e.g., to achieve high temperature stability or lower hardness) [64]. Metal coatings are preferably used when fiber applications are envisioned under harsh conditions (e.g., aggressive media, mechanical impacts), or when special properties are necessary (e.g., rapid fiber cooling during fiber operation) [65].

Furthermore, other inorganics such as carbon coatings can be applied to obtain a hermeticity (against hydrogen and/or moisture or liquid water) that cannot otherwise be achieved. Carbon layers on silica also influence surface properties such as wettability, which is of great importance for additional organic or metallic layers [66].

The coatings all differ in their physicochemical properties such as refractive index, elastic modulus, elongation, hardness, water and hydrogen permeability, glass transition temperature, and thermal stability. The suitability of the coating strongly depends on the targeted application of the final fiber. The selection of the appropriate coating formulation asks for a detailed analysis of the envisioned application in terms of environmental conditions, planned measurement methods/analysis of fibers, and of course simple handling aspects (i.e., local/temporal removability of coating).

An overview of chemical and optical properties of selected fiber coatings is shown in Table 5.

Basic coating formulations usually need to be specifically adapted for in-line application during fiber drawing

Table 5 Chemical and optical properties of selected fiber coatings listed according to decreasing refractive index.

	Curing	Viscosity (uncured)[a] [Pas]	n (cured)[b]	NA[c]	Max. coating thickness[d] (µm)
Polyamidimide	T	n.a.	1.81		6
Polyimide (Microquartz)	T	26.2	1.68		7
Polyimide (PMGI)	T	9.8	1.57		6
ORMORCER®	UV	3.0	1.51		100
Urethane-Acrylate DSM 3471-3-14	UV	9.2	1.505		100
Silica			1.4469		
Silicone LR7665 (Wacker)	T	14.2	1.415	0.30	100
Silicone RT601 (Wacker)	T	2.9	1.409	0.33	100
F-Acrylate Opticlad	UV	3.2	1.38	0.43	50
F-Acrylate (SSCP) PC 373	UV	3.5	1.376	0.45[e]	60
F-Acrylate (SSCP) PC 370	UV	5.7	1.372	0.46	60
F-Acrylate (SSCP) PC 363	UV	5.0	1.363	0.49	60
OF-133 (MyPolymers)	UV	n.a.	1.326	0.61[e]	50
Teflon AF (Du Pont)	T	n.a.	1.314	0.61	3

[a]25°C, [b]measured at 1300 nm (prism coupling device), [c]calculated from n, [d]single layer, depending on required layer properties (e.g., bubble-free) and technology (dip coating vs. pressure coating), [e]measured using far field method.

(see, for example, [67–69]). Numerous commercially available coating formulations exist. Specific additives, such as photoinitiators, adhesion promoters, inhibitors, antioxidants, or solvents, might be necessary to adjust the viscosity and facilitate the high-speed in-line coating process. Some of the general coating material requirements for in-line application are summarized in Table 6.

Furthermore, the available drawing tower equipment must be respected and might limit the choice. Coating and curing conditions need to be carefully checked before proceeding to the in-line coating process of the fiber.

The quality of the cured fiber coating is usually verified using optical methods (microscopy, absorption, and spectral loss), mechanical testing (modulus of rupture of coated fiber), and hermeticity testing (hydrogen and water absorption test).

The common in-line coating application process for polymers or hybrid materials is either gravity coating or pressure coating. The simplest method of the two is gravity coating using a conically-shaped coating die. This method is convenient in terms of setup and handling during drawing, and it allows for fiber diameter adjustment at the beginning of the drawing process, but there are always air bubbles entrapped in the coating reservoir due to the drawing dynamics, and there is always a risk of dust particle contamination decreasing coating quality. To circumvent these drawbacks, a pressurized coating system is preferred. Due to the external pressure within the coating vessel, the dynamics of the coating system (e.g., shear) are advantageously changed, and very high quality coatings are obtained. However, the pressurized coating system demands extensive cleaning effort and more coating material due to dead volumes within the lines of the setup.

Several simulations of the coating process and coating thicknesses obtained are available in literature for open coating applicator setups and pressurized coating applicators [61, 70–74]. Detailed modeling work and a comparison to practical results were conducted in Jaluria et al. [75–78]. Coating thickness fluctuations [79], special

Table 6 General material requirements for the dynamic coating of fibers.

Liquid state	Surface tension	N/m	0.02–0.2
	Viscosity	Pa s	1–10
	Curing		thermal or UV
	Curing time	Sec	0.1–2.5
	Solvent content		as low as possible
	Shrinkage during curing		as low as possible
	Polymerization		preferably without water generation
Cured state	Layer thickness of cured material (single coating)	µm	≤50
	Young's modulus of cured material	GPa	≤1.5

coating process effects (e.g., coating concentricity) [80], slip [81], and thermally induced stresses [82] have also been addressed.

The thickness of the gravity coating during the drawing process can be derived mathematically based upon the Hagen-Poisseuille equation, and the assumption of ideal flow (laminar flow, Newtonian liquid). An approximate estimation results in the following simplified equation 3, [61, 74], which neglects shrinkage during curing.

$$s = h - a = \sqrt{\frac{R^2 - a^2}{2\ln\left(\frac{R}{a}\right)}} - a \tag{3}$$

where s is the final coating thickness, h is the radius of the coated fiber, a is the fiber radius, and R is the radius of the coating die cross section.

In practice, drawing parameters particularly effect the viscous flow behavior of the coating material in the coating die, thus yielding a somewhat different final coating thickness. Exemplary data from fiber drawing experiments and the prediction according to the simplified model, equation 3, are plotted in Figure 12.

Usually, a polymer or hybrid coating thickness of about 50 μm is sufficient for fiber strength preservation. In some cases, lower thicknesses (as low as 5 μm or even lower) may be sufficient (e.g., for Teflon coatings or polyimides).

3.3 Speciality fibers

A wide range of specialty fibers exists for different applications. In the next section, we will discuss two classes of such fibers that have been the focus of special research interest during recent years: microstructured fibers (MOFs) and hybrid fibers. These fiber types enable propagation properties well beyond the properties of more conventional core-cladding fiber structures.
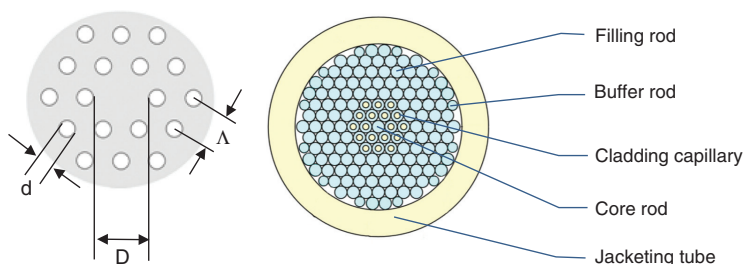
Figure 12 Coating thickness as a function of the drawn fiber diameter and coating die diameter. Solid lines: simplified model (see equation 3). Squares: experimental values. Black: 195 μm coating die diameter; red: 345 μm coating die diameter; blue: 600 μm coating die diameter.

3.3.1 Microstructured fibers prepared by stack and draw technique

The concept of microstructured fibers (MOFs), pioneered in 1996 by Russell et al. [83], allows a wide variety of applications due to a large amount of freedom in the design of the arrangement of doped or undoped capillaries and rods. MOFs with different light-propagating mechanisms are widely described in review articles [84, 85]. Depending on their structural design, MOFs are operated by the photonic band gap effect or by total internal reflection (TIR). In this section, we concentrate on MOFs operated via TIR. They typically have a solid central core with a diameter D that acts like a compact structural defect in a hexagonal holey arrangement with a uniform pitch size Λ and a hole diameter d (see Figure 13, left). This holey cladding is usually arranged as a multiple number of capillary rings.

The common technology used in the preparation of MOFs is the drawing of capillary and rod composed preforms, often referred to as the stack-and-draw technique. Rods and capillaries with uniform outer diameters are

Figure 13 Principle profile of a MOF (also: holey fiber) operating in TIR with two capillary rings (left: geometric parameters, right: scheme of arrangement of the packing elements).
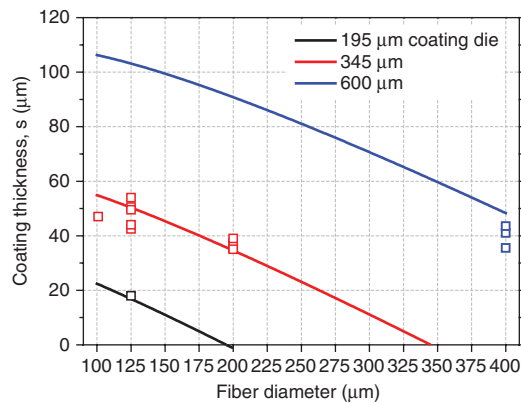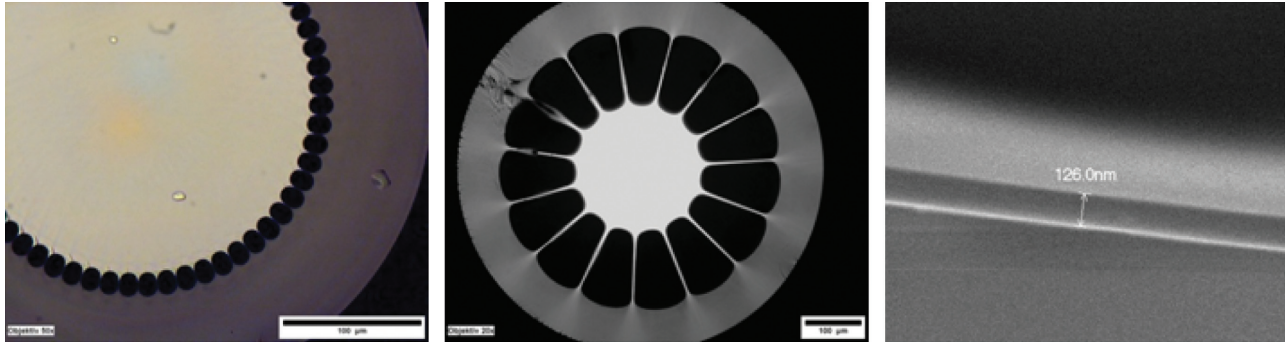
Figure 14 Micrographs of the air-clad fibers with different capillary stretching ratios (left, middle) and an SEM image of an air-clad bridge (right).

typically arranged in a hexagonal package and cladded with a jacketing tube. To span the mismatch between the hexagonal arrangement and the circular outer tube, buffer rods with different diameters are often used to fill the interstitial volume. Figure 13 (right) shows a typical preform package arrangement. Two TIR MOF types with high practical relevance are discussed in the following: air-clad fibers and suspended-core fibers.

Air-clad fibers: One outstanding feature of MOFs is the feasibility of achieving a high numerical aperture, NA, >0.6. High effective index differences between guided core modes and cladding modes are possible due to the high refractive index contrast between the silica and air of about 0.45 when implementing a high air fraction and small bridge widths in the air clad. Such fibers are suitable for optical power or signal transmission, or for refractive index sensing, mostly in the multi-mode light propagation regime [86]. Air-clad fibers are manufactured using the stack-and-draw technique. Core rod and air-clad capillaries with a typical outer diameter of 1 mm and the overcladding tube are typically made from synthetic silica (e.g., Heraeus Suprasil F300). The capillaries are inserted into the ring-shaped air space between the silica core rod and the overcladding tube. For a high NA in the final fiber, a very small bridge thickness of <1 μm is required. Simulations show the importance of a very small bridge thickness [87]. Figure 14 shows the micrographs of prepared air-clad fibers with different core diameters and air-clad designs. The capillaries and the ring-shaped interface of the preform are connected with a pressurizing system. The inner capillary volume is pressurized, whereas the interstitial volume between the core and overcladding tube is weakly evacuated. Simulations to control the combined stretching and inflating process of the capillaries during drawing are described in [88].

By stretching the capillaries through overpressure, the bridge width, w, can be narrowed in the range of a tenth of a micrometer see Figure 14, right). In terms of the much smaller dimensions compared to the operating wavelength (λ≈1 μm), a numerical aperture of about 0.9 can be achieved (Figure 15).

Suspended core fibers: Suspended core fibers (SCFs) are a specific type of MOF with extremely small cores and relatively large cavities. They are of particular interest for nonlinear applications due to the small core diameter and large NA, e.g., for supercontinuum generation or RAMAN amplification. Such fibers are also suitable for the evanescent sensing of fluid media in chemical engineering and for environmental monitoring or biological investigations by filling the cavities with liquid or gaseous analytes. SCFs with three and four bridges were prepared as a preform by arranging thin-walled capillaries (silica F300) in an overcladding tube. This package is then drawn to a fiber. By applying overpressure in the cavities, the bridge width can be controlled. Compared to the air-clad fibers (see Figure 14) and holey structures shown in Figure 13, in SCFs the core is usually formed by the coalescence of the three or four capillaries. The three-cavity fiber in Figure 16A has
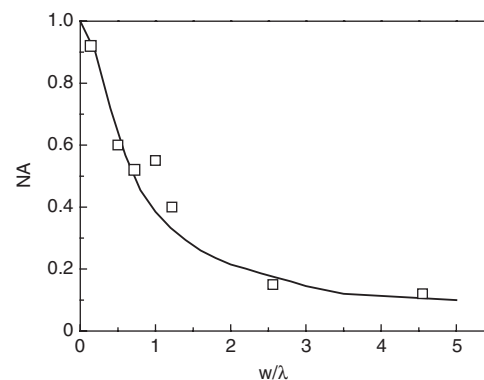

Figure 15 Effect of the bridge width, w, on the numerical aperture, NA. The solid line follows the simulations in [85].
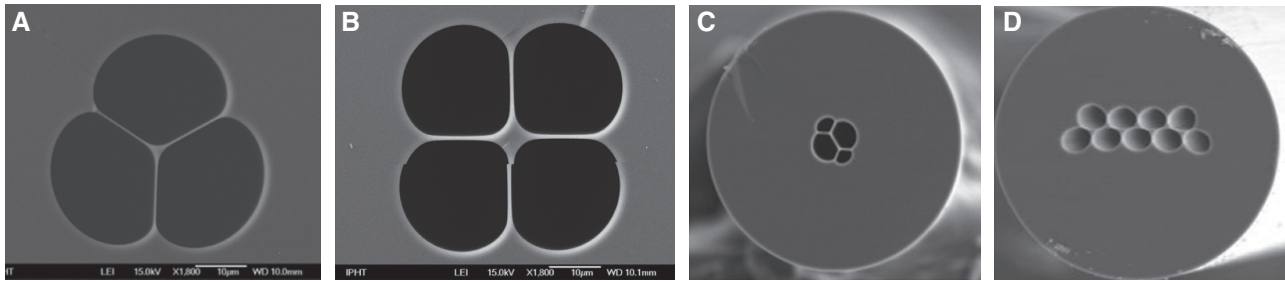
Figure 16 SEM micrographs of three and four-cavity SCFs and suspended multi-core fibers.

a bridge width of about 0.8 μm; the four-cavity fiber in Figure 16B has a bridge width of 0.5 μm. These examples show that a bridge thickness smaller than the typically used wavelength is possible.

Another type of SCF is the suspended multi-core fiber. Here, a number of cores are suspended, allowing the temperature and strain-independent interferometric sensing of torsion effects (Figure 16C), or the simultaneous measurement of curvature and strain (Figure 16D) via interaction of the light guided in the different cores [89, 90].

The effective core diameters in the fibers shown are 1.3 μm (Figure 16A) and 5.0 μm (Figure 16B). The small core diameter ensures a high evanescent mode-field overlap in the capillary cavities (e.g., for the NIR absorption sensing of hydrocarbons) [91]. The numerical apertures are 0.68 and 0.50, respectively. The suspended twin core fiber (Figure 16C) shows core sizes of 1.5 μm and a core distance of 7.6 μm, where sensing is based on the differential optical path of the light in the two cores associated with a refractive index difference of about 10^{-3} [89]. Using the suspended seven-core fiber (Figure 16D), the spectral response is based on complex interference patterns. The core sizes are comparable to the twin core fiber, and the core distance is 9.2 μm [89]. The typical loss spectrum of a suspended core fiber with a minimum loss of <15 dB/km is shown in Figure 17.

3.3.2 Non-silica and hybrid fibers based on melt glasses and rod-in-tube technology

One approach to taking advantage of the superior properties of silica glass and the extended solubility of RE (active materials) and higher nonlinearity (passive materials) of lanthanum-containing silicate glasses is the fabrication of hybrid fibers. Here, different materials are combined as a core and cladding which are not compatible in their thermo-mechanical properties. Such a combination is,
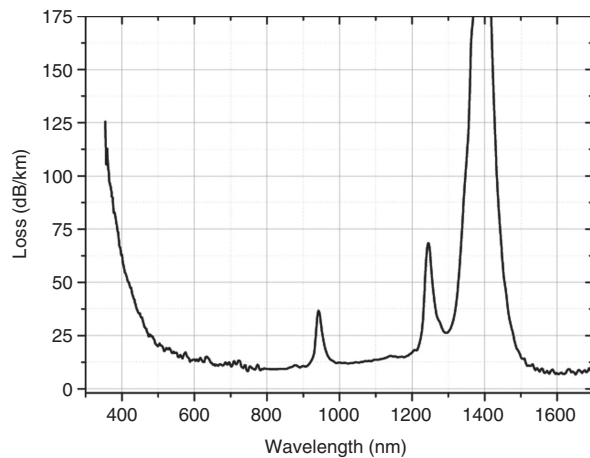

Figure 17 Attenuation spectrum of the three-cavity SCF.

for example, of interest if an active core material optimized for nonlinearity or lasing efficiency is integrated into a silica glass cladding structure with its passive and mechanical optical properties. Several approaches are available for the fabrication of hybrid fibers, such as the high pressure filling technique of capillary fibers and MOFs [92, 93] or the simultaneous drawing of different glass types [47, 48]. High pressure filling allows the combination of a greater variety of materials but only for short fiber lengths of several tens of centimeters. The direct drawing process results in much higher fiber lengths but is applicable for a lower diversity of combinable materials only.

As described in section 4, SAL glass preforms were prepared based on molten glasses. In the same way, cladding tubes were also prepared with an additional hole drilling. Fibers with a SAL glass cladding and core (Figure 18A) have been produced using rod-in-tube (RIT) technology. Replacing the SAL glass cladding tube with silica produces a so-called hybrid fiber (Figure 18B). Depending on the required fiber cross section (increase in the cladding-core-diameter ratio (CCDR), the preforms have been drawn to canes of 2–3 mm in diameter, followed
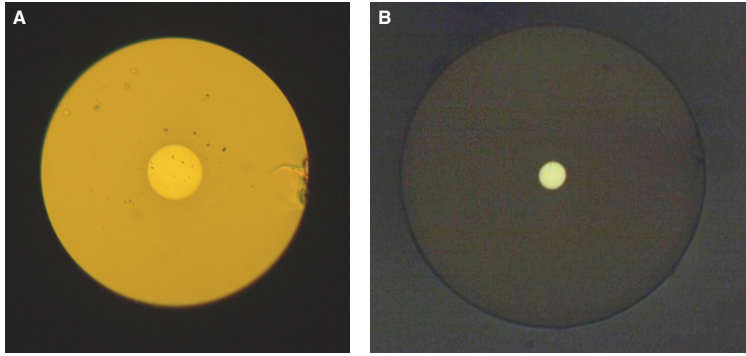
Figure 18 Structured fiber with SAL glass core and cladding (A), structured hybrid fiber with SAL glass core and silica glass cladding (B).

by an additional RIT drawing step to form the final fiber (Figure 18B).

In such a hybrid fiber preparation procedure, several aspects are very challenging: i) the viscosity of the two glasses during fiber drawing differs by at least two orders of magnitude, ii) the expansion coefficient of the SAL glass is at least eight times higher than that of silica (4 ppm/K vs. 0.5 ppm/°K), and iii) temperature-dependent phase separations can occur. In the SiO_2-Al_2O_3 system, phase separation depends on the aluminum oxide content and the temperature [49]. In the material system described, phase separation can be enhanced by two additional processes: codoping (e.g., with lanthanum or ytterbium), and the material flow/diffusion of SiO_2 from the silica cladding.

In particular, the potential phase separation at high silica concentrations has implications for the fiber drawing process and limits the possible number of high temperature processing steps. Also, if the diffusion and material flow effects enrich the core-cladding interface region with SiO_2, phase separation becomes very likely.

Accordingly, important considerations for a hybrid fiber fabrication process include the following: i) minimizing the preform dwell time in the drawing furnace hot zone (this requires small diameter preforms to reduce the preform-to-fiber elongation ratio), ii) limiting the number of hot processing steps, and iii) optimizing the core glass composition to compensate possible diffusion processes and to suppress phase separation.

As can be seen from Figure 19, the hybrid fibers show almost the same spectral attenuation properties as the pure SAL glass fiber. No additional losses are introduced by the interface of different materials. However, measurements of the numerical aperture have shown values with a maximum of 0.54, which is lower than the theoretically expected values of 0.8. This is due to the diffusion processes of SiO_2 into the SAL glass core during fiber fabrication as mentioned above.
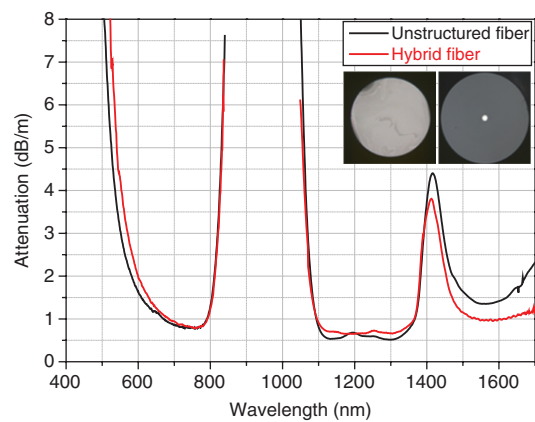

Figure 19 Comparison of fiber losses of a pure SAL glass fiber and a hybrid fiber (silica cladding SAL glass core).

4 Conclusions

The attractive application options of modern optical fibers have initiated many material and process-oriented innovations in the field of glass technology. Today, extreme properties in optical fibers concerning purity, homogeneity, or structural sizes have been achieved which allow not only optimized performance in communication applications but also enable further challenging applications, such as fiber amplifiers and fiber lasers or as miniaturized and distributed sensor elements. We have presented an overview of advanced conventional technologies and innovative new concepts for the preparation of materials and fiber preforms. The advances achieved will certainly improve the versatility of the fiber optical guiding concept (e.g., for fibers with integrated functionality) and will also be attractive for other glass-based optical applications, such as special solid-state lasers, nonlinear optical glasses, structured glass elements, and specialized optical elements.

References

[1] T. Miya, Y. Terunuma, T. Hosaka, T. Miyashita, Electron. Lett. 15, 106–108 (1979).

[2] F. Benabid, Phil. Trans. R. Soc. A 364, 3439–3462 (2006).

[3] H. Zhang, H. Xiao, P. Zhou, X. Wang, X. Xu, IEEE Photon. Technol. Lett. 25, 2093–2096 (2013).

[4] C. Farrell, K. A. Serrels, T. R. Lundquist, P. Vedagarbha, D. T. Reid, Opt. Lett, 37, 1778–1780 (2012).

[5] E. Cibula, S. Pevec, B. Lenardič, É. Pinet, D. Donlagić, Opt. Exp. 17, 5098–5106 (2009).

[6] J. Ballato, P. Dragic, J. Am. Ceram. Soc., 96, 2675–2692 (2013).

[7] P. Shukla, J. Lawrence, Optics & Laser Technol. 54, 380–388 (2013).

[8] P. St. J. Russell, Science 299, 358–362 (2003).

[9] C. Valentin, P. Calvet, Y. Quiquempois, G. Bouwmans, L. Bigot, et al., Opt. Exp. 21, 23250–23260 (2013).

[10] X. Feng, A. K. Mairaj, D. W. Hewak, T. M. Monro, J. Lightw. Technol. 23, 2046–2054 (2005).

[11] G. Vienne, Y. Xu, C. Jakobsen, H.-J. Deyerl, J. B. Jensen, et al., Opt. Exp. 12, 3500–3508 (2004).

[12] F. Tosco, Fiber Optics Communication Handbook, CSELT, TAB Professional and Reference Books (1990).

[13] J. Mac Chesney, D. J. DiGiovanni, J. Am. Ceram, Soc. 73, 3527–3556 (1990).

[14] T. Izawa, IEEE J. on Selected Topics in Quantum Electronics 6, 1220–1227 (2000).

[15] S. R. Nagel, J. B. Mac Chesney, K. L. Walker, IEEE J. Quantum Electron. QE-18, 459–476 (1982).

[16] J. Kirchhof, S. Unger, J. Non-Cryst. Solids 354, 540–545 (2008).

[17] J. Kirchhof, S. Unger, B. Knappe, Adv. Mat. Res. 39–40, 265–268 (2008).

[18] J. Kirchhof, S. Unger, K.-F. Klein, B. Knappe, J. Non-Cryst. Solids 181, 266–273 (1995).

[19] J. Kirchhof, S. Unger, J. Dellith, J. Non-Cryst. Solids 345–346, 234–238 (2004).

[20] J. Kirchhof, S. Unger, B. Knappe, J. Dellith, Phys. Chem. Glasses 48, 129–133 (2007).

[21] J. Kirchhof, S. Unger, J. Dellith, A. Scheffel, Ch. Teichmann, Opt. Mat. Exp. 2, 534–547 (2012).

[22] J. E. Townsend, S. B. Poole, D. N. Payne, Electron. Lett. 23, 329–331 (1987).

[23] J. Kirchhof, S. Unger, A. Schwuchow, Proc. SPIE 4957, 1–12 (2003).

[24] S. Unger, J. Dellith, A. Scheffel, J. Kirchhof, Phys. Chem. Glasses: Eur. J. Glass Sci. Technol. B 52, 41–46 (2011).

[25] S. Unger, A. Schwuchow, J. Dellith, J. Kirchhof, Proc. SPIE 6469, 646913 (2007).

[26] S. Unger, A. Schwuchow, S. Jetschke, V. Reichel, A. Scheffel, et al., Proc. SPIE 6890, 6890016 (2008).

[27] J. Kirchhof, S. Unger, S. Jetschke, A. Schwuchow, M. Leich, et al., Proc. SPIE 7195, 71950S (2009).

[28] J. Kirchhof, S. Unger, A. Schwuchow, S. Jetschke, V. Reichel, et al., Proc. SPIE 7598, 75980B/1-11 (2010).

[29] S. Unger, A. Schwuchow, S. Jetschke, St. Grimm, A. Scheffel, et al., Proc. SPIE 8621, 862116 (2013).

[30] A. Popp, A. Voss, Th. Graf, S. Unger, J. Kirchhof, et al., Laser Phys. Lett. 8, 887–894 (2011).

[31] S. Jetschke, S. Unger, A. Schwuchow, M. Leich, J. Kirchhof, Opt. Exp. 16, 15540–15545 (2008).

[32] S. Jetschke, M. Leich, S. Unger, A. Schwuchow, J. Kirchhof, Opt. Exp. 19, 14473–14478 (2011).

[33] S. Jetschke, S. Unger, M. Leich, J. Kirchhof, Appl. Opt. 51, 7758–7764 (2012).

[34] S. Jetschke, A. Schwuchow, S. Unger, M. Leich, M. Jäger et al., Opt. Mat. Exp. 3, 452–458 (2013).

[35] S. Jetschke, S. Unger, A. Schwuchow, M. Leich, J. Fiebrandt, et al., Opt. Exp. 21, 7590–7598 (2013).

[36] R. P. Tumminelli, B. C. McCollum, E. Snitzer, J. Lightw. Technol. 8, 1680–1683 (1990).

[37] A. J. Boyland, A. S. Webb, S. Yoo, F. H. Mountfort, M. P. Kalita, et al., J. Lightw. Technol. 29, 912–915 (2011).

[38] M. M. Bubnov, V. N. Vechkanov, A. N. Guryanov, K. V. Zotov, D. S. Lipatov, et al., Inorg. Mat. 45, 444–449 (2009).

[39] E. H. Sekiya, P. Barua, K. Saito, A. J. Ikushima, J. Non-Cryst. Solids 354, 4737–4742 (2008).

[40] S. Saha, A. Pal, R. Sen, IEEE Photon. Techn. Lett. 26, 58–61 (2014).

[41] S. Unger, F. Lindner, C. Aichele, M. Leich, A. Schwuchow, et al., Laser Phys. 14, 035103/1–5 (2014).

[42] A. Langner, M. Such, G. Schötz, V. Reichel, St. Grimm, et al., Proc. SPIE 7580, 758015 (2010).

[43] M. Leich, F. Just, A. Langner, M. Such, G. Schötz, et al., Opt. Lett. 36, 1557–1559 (2011).

[44] A. Langner, M. Such, G. Schötz, F. Just, M. Leich, et al., Proc. SPIE 8601, 8601OG (2013).

[45] M. Loeser. F. Röser, A. Reichelt, M. Siebold, S. Grimm, et al., Opt. Lett. 37, 4029–4031 (2012).

[46] K. Schuster, J. Kobelke, D. Litzkendorf, A. Schwuchow, F. Lindner, et al., Proc. SPIE 7934, 79340O (2011).

[47] M. J. Hyatt, D. E. Day, J. Am. Ceram. Soc. 70, C283–C287 (1987).

[48] J. E. Shelby, Key Eng. Mat., Vol. 94–95, Trans Tech Publications, Switzerland (1994).

[49] M. J. Dejneka, B. Z. Hanson, S. G. Crigler, L. A. Zenteno, J. D. Minelly, et al., J. Am. Ceram. Soc. 85, 1100–1106 (2002).

[50] D. Litzkendorf, S. Grimm, K. Schuster, J. Kobelke, A. Schwuchow, et al., Int. J. Appl. Glass Sci. 3, 321–331 (2012).

[51] S. Kuhn, A. Herrmann, J. Hein, M. C. Kaluza, C. Rüssel, J. Mater. Sci. 48, 8014–8022 (2013).

[52] S. Rehkson, J. Leonard, P. Sanger, Am. Ceram. Soc. Bull. 6, 9401–9407 (2004).

[53] H. A. Aulich, J. G. Grabmaier, K. H. Eisenrith, Appl. Opt. 17, 170–171 (1978).

[54] E. M. Dianov, V. V. Kashin, S. M. Perminov, V. N. Perminova, S. Y. Rusanov, et al., Glass Technol. 29, 258–262 (1988).

[55] X. Cheng, Y. Jaluria, Numer. Heat Tr. A-Appl. 41, 757–781 (2002).

[56] U. C. Paek, R. B. Runk, J. Appl. Phys. 49, 4417–4422 (1978).

[57] U. C. Paek, C. R. Kurkjian, J. Am. Ceram. Soc. 58, 330–335 (1975).

[58] K. J. Lyytikäinen, PhD Thesis, Chapter 6.3.5. "Furnace design" 202–204, Sydney, (2004).

[59] U. C. Paek, C. M. Schroeder, C. R. Kurkjian, Glass Technol. 29, 263–266 (1988).

[60] S. R. Schmid, A. F. Toussain, in Optical Fiber Coatings, Chapter 4 in Specialty Optical Fibers Handbook. Ed. A. Méndez, T. F. Morse. Academic (Press Elsevier, 2007) pp. 95–122.

[61] U. C. Paek, J. Lightw. Technol. 4, 1048–1060 (1986).

[62] L. L. Blyler, F. V. DiMarcello, Proc. IEEE. 68, 1194–1198 (1980).

[63] L. L. Blyler, F. V. DiMarello, D. H. Smithgall, U. C. Paek, Tech. Dig. OFC'1983 (New Orleans, LA), 1983, TuF1.

[64] K. Schuster, J. Kobelke, K. Rose, M. Helbig, M. Zoheidi, et al., Proc. SPIE 7598, P. Soc. Photo-Opt. Ins., 75980H (2010).

[65] V. A. Bogatyrev, S. Semjonov, Metal-coated fibers. Chapter 15 in Specialty Optical Fibers Handbook. Ed. A. Méndez, TF Morse. Academic (Press Elsevier, 2007) pp. 491–512.

[66] P. J. Lemaire, E. A. Lindholm, Hermetic optical fibers: Carbon-coated fibers. Chapter 14 in Specialty Optical Fibers Handbook. Ed. A. Méndez, TF Morse. Academic (Press Elsevier, 2007) pp. 453.

[67] F. Masson, C. Decker, S. Andre, X. Andrieu, I. Acrylic resins. Progr. Org. Coat. 49, 1–12 (2004).

[68] W. Z. Wang, K.X. Cheng, Eur. Polym. J. 39, 1891–1897 (2003).

[69] H. D. Kim, S. G. Kang, C. S. Ha, J. Appl. Pol. Sci. 46, 1339–1351 (1992).

[70] U. C. Paek, J. Heat Transf.-Trans. ASME. 121, 774–788 (1999).

[71] S. Ravinutala, C. Polymeropoulos, Exp. Thermal Fluid Sci. 26, 573–580 (2002).

[72] C. Y. Zhao, S. H. K. Lee, J. Mat. Process. Manuf. Sci. 8, 53–73 (1999).

[73] A. Panoliaskos, W. L. H. Hallett, I. Garis, Appl. Opt. 24, 2309–2312 (1985).

[74] U. C. Paek, C. M. Schroeder, Fiber Integr. Opt. 2, 287–298 (1979).

[75] S. Y. Yoo, Y. Jaluria, Numer. Heat Tr. A-Appl. 53, 111–131 (2008).

[76] S. Y. Yoo, Y. Jaluria, Int. J. Heat Mass Transf. 50, 1176–1185 (2007).

[77] S. Y. Yoo, Y. Jaluria, J. Lightw. Technol. 24, 449–463 (2006).

[78] K. Rattan, Y. Jaluria, Comp. Mech. 31, 428–436 (2003).

[79] Q. B. Jiang, F. Z. Yang, R. Pitchumani, J. Lightw. Technol. 23, 1261–1272 (2005).

[80] D. Marcuse, H. M. Presby, Appl. Opt. 16, 2383–2390 (1977).

[81] M. Wagatsuma, T. Kimura, S. Aymakawa, J. Lightw. Technol. 4, 1414–1419 (1986).

[82] W. W. King, J. Lightw. Technol. 9, 952–953 (1991).

[83] J. C. Knight, T. A. Birks, P. St. J. Russell, D. M. Atkin, Opt. Lett. 21, 1547–1549 (1996).

[84] P. S. J. Russell, Science 299, 358 (2003).

[85] J. C. Knight, Nature 424, 847 (2003).

[86] S. Silva, J. L. Santos, F. Xavier Malcata, J. Kobelke, K. Schuster, O. Frazão, Opt. Lett. 36, 852–854 (2011).

[87] N. A. Issa, Appl. Opt., 43, 6191–6197 (2004).

[88] J. Kirchhof, J. Kobelke, K. Schuster, H. Bartelt, R. Iliew, et al., Chapt.: 14 Photonic Crystal Fibers in Photonic Crystals: Advances in Design, Fabrication, and Characterization. Ed. by Kurt Busch, Stefan Lölkes, Ralf B. Wehrspohn, Helmut Föll, (Wiley-VCH Verlag GmbH & Co. KGaA, 2004) pp. 266–288.

[89] O. Frazão, R. M. Silva, J. Kobelke, K. Schuster, Opt. Lett. 35, 2777–2779 (2010).

[90] R. M. Silva, M. S. Ferreira, J. Kobelke, K. Schuster, O. Frazão, Opt. Lett. 36, 3939–3941 (2011).

[91] H. Lehmann, J. Kobelke, K. Schuster, A. Schwuchow, R. Willsch, et al., Proc. SPIE 7004, 70042R (2008).

[92] P. D. Dragic, T. Hawkins, P. Foy, S. Morris, J. Ballato, Nature Photonics 6, 627–633 (2012).

[93] J. Ballato, T. Hawkins, P. Foy, B. Kokuoz, R. Stolen, et al., J. Appl. Phys. 105, 0533110/1–9 (2009).

Kay Schuster holds the group leader position of the Optical Fiber Technology Group within the Fiber Optics Division. Beside the fabrication of specialty microstructured fibers the group is intensively engaged in material science as well as preform and fiber manufacturing for high power fiber lasers and FBG and Raman based sensing applications. Complex structures of high silica and silicate glass based fibers have been realized for the development very large mode area laser fibers. In the applicative critical field of special sensor fibers for high temperature applications he is intensively engaged in the application and alignment of suitable fiber coating materials (e.g., ORMOCER®s, siloxanes, polyimides, metals).

Sonja Unger works at the IPHT as a research collaborator in the field of MCVD technology. She is engaged in the development of materials and high silica specialty optical fibers. Her recent activities are focused on investigations on active fibers for laser and amplifier as well as photosensitive fibers for the fabrication of Draw Tower Gratings DTG®.

Claudia Aichele is a member of the Optical Fiber Technology Group at IPHT and works as an engineer for material science in the field of doped silica glasses and optical fibers. For the last 13 years, she has been involved in the development of gas phase deposition methods like flame hydrolysis deposition, direct melting technique, and MCVD for the preparation of planar optical waveguides and specialty optical fibers. Recently she has been focussing on the incorporation of RE elements and aluminum in silica glass with a gas phase doping technique combined with the MCVD method for special laser fibers.

Florian Lindner is an engineer for material science and PhD student working in the field of MCVD technology. He is engaged in the development of materials and gas phase deposition method for the preparation of specialty optical fibers. His current research focuses on incorporation of RE elements and aluminum in silica glass with a gas phase doping technique combined with the MCVD method for special laser fibers.

Stephan Grimm is chemist and specialized in the field of glass chemistry. Since 1995 he works in the field of optical fibers fabricated by the MCVD-Process. He is currently engaged in preparation of RE doped laser fiber materials. He is significantly involved in the development of a new powder sinter process (REPUSIL) for the fabrication of doped bulk silica glass for special fiber lasers like LMA-type fiber and rod type fiber.

Doris Litzkendorf received her Diploma degree in Chemistry in 1984 from the University of Jena, Germany. From 1984 to 1989, she was with the Otto Schott Institute for Glass Chemistry, University of Jena, working on new photochromic glasses. From 1989 to 2006 she worked at the Magnetics Department of Institute for Physical High Technology Jena in the field of material science. Since 2007, she is member of the Optical Fibers Technology Group within the Fiber Optics Division at the Leibniz Institute of Photonic Technology in Jena. Her current research focuses on the development of RE doped silicate glasses and fibers for laser and nonlinear applications.

Jens Kobelke works at IPHT Jena on development and preparation of special optical fibers based on different glass materials (e.g., chalcogenide glasses, HMO glasses, high silica). He is engaged in preparation and characterization of microstructured fibers based on high silica and other glass materials.

Jörg Bierlich worked as a graduate engineer at the IPHT Jena in the Department of Magnetics from 2001 to 2008. During 2005–2008 he studied at the University of Technology "Bergakademie" Freiberg and received his PhD focused on superconducting ceramic composites. Since 2008 he has been working at the IPHT Jena in the department of Fiber Optics in the field of fiber drawing technologies and the development of special optical fibers and is engaged in the preparation and characterisation of microstructured fibers based on high silica and other glass materials.

Katrin Wondraczek has been working in the Optical Fiber Technology Group since 2012. Her focus is on drawing and coating of optical specialty fibers. After receiving her PhD in Physical Chemistry in 2005 she joined Corning S.A.S. in France to work on functionalized glass coatings. Prior to her engagement at the Leibniz IPHT, she was employee of AREVA GmbH, Erlangen, being in charge of chemical metal surface treatment.

Hartmut Bartelt is Professor for Modern Optics at the University of Jena (Germany) and Head of the Fiber Optics Research Department at the Leibniz Institute of Photonic Technology (IPHT). His research activities cover the fields of optical specialty fibers, micro and nano-structured fiber optics, fiber light sources, fiber Bragg gratings and fiber optical sensors.